Ab Initio Time-Domain Study of Phonon-Assisted Relaxation of Charge Carriers in a PbSe Quantum Dot

Svetlana V. Kilina, Colleen F. Craig, Dmitri S. Kilin, and Oleg V. Prezhdo*

Department of Chemistry, University of Washington, Seattle, Washington 98195-1700

Received: October 20, 2006; In Final Form: December 25, 2006

The phonon-induced relaxation dynamics of charge carriers in a PbSe quantum dot is studied for the first time by ab initio density functional theory in the time-domain. The picosecond time scale of the relaxation and the absence of the phonon bottleneck are rationalized by relatively high electron and hole state densities. While many of these states show only weak optical activity, most of them participate in the electron-vibrational relaxation. Our simulations demonstrate that the slight asymmetry in the electron and hole band structure is sufficient to allow symmetry-forbidden S−P, P−S, etc. transitions, which are seen in the experimental absorption spectra. The relaxation is nonexponential, in agreement with the strongly non-Lorentzian spectral line shapes observed in experiments. The energy exchanged during individual transitions is typically greater than the characteristic phonon energy, indicating that the transitions are multiphonon. Both electrons and holes interact better with low-frequency acoustic phonons, rather than higher frequency optical modes. Holes decay only slightly faster than electrons, rendering the hole-assisted Auger relaxation pathways inefficient. This relatively symmetric vibrational relaxation of electrons and holes proceeds on a picosecond time scale, much slower than the ultrafast highly efficient carrier multiplication that was reported recently in relation to improved solar power conversion.

1. Introduction

Nanometer-size crystals of inorganic semiconductors, known as artificial atoms or quantum dots (QD), exhibit a variety of unique properties that can be controlled not only by the type of material, but also by the size, shape, and topology of the nanocrystal.[1] The new types of physical processes available in QDs motivate their application in spintronics[2] and quantum computing.[3,4] QDs have been incorporated into thermopower[5] and photovoltaic[6−12] devices, lasers,[12,13] field-effect transistors,[14] light-emitting diodes,[15] quantum emitter antennas,[16] and fluorescent biological imaging probes.[17] The QD response to various external perturbations that are used to activate and utilize the QD properties greatly depends on the details of excitation, charge, and phonon dynamics, which are intimately intertwined and cover a range of time scales and mechanisms. The phonon-mediated relaxation of electrons and holes in QDs is the focus of many experimental[6−11,18−26] and theoretical[18,27−30] efforts, and plays a crucial role in a variety of applications. For instance, the electron−phonon relaxation rates determine the efficiency of QD-based lasers[12,13] and photovoltaic devices.[6−12] QD application to quantum information processing[2−4,16] is limited by the phonon-induced dephasing of electron[29,30] and spin[24,27] excitations. Electron−phonon interactions define linewidths of QD optical spectra.[20,26,30] Inelastic electron−phonon scattering modulates electron tunneling transport through QDs and is responsible for transport blockade and energy loss.[25] Electron−phonon coupling forms the basis of laser cooling of nanomechanical resonator modes in an embedded QD.[28] While a variety of time-resolved experimental techniques are extensively used to probe the features of the charge-phonon dynamics in QDs,[6−11,18−26] current theoretical approaches focus on characterization of QD structure and spectra,[7,18,27−36] with few efforts devoted to direct real-time modeling of the experimental data.

Of all the semiconducting nanomaterials studied in the past few years, lead salts, such as PbS and PbSe, show some of the most unique electronic and transport properties.[37−41] In contrast to other semiconductors, the nanocrystals of PbSe and PbS have nearly symmetric conduction band (CB) and valence band (VB) at the direct gap and, correspondingly, similar effective masses of the electron and hole.[42] As a result, the Auger relaxation processes are inefficient when compared to a nanocrystal with asymmetric CB and VB, such as CdSe, in which the Auger-type electron−hole energy transfer opens up a new relaxation channel.[21] The effective masses of electrons and holes in lead salts are not only similar, they are also small, promising strong quantum confinement effects[37] and inducing quantization of bulk electronic bands. The discrete electronic energy spectrum of QDs has a profound impact on the phonon−carrier interaction, since the condition of matching the phonon and electron energy gaps can be much harder to satisfy. A mismatch between the electronic and vibrational energy quanta is expected to produce a phonon bottleneck in the charge-carrier relaxation.[6] A significant phonon bottleneck, coupled with low rates of Auger-type cooling, favors carrier multiplication in PbSe and PbS nanostructures. Recent time-resolved experiments[7−11] demonstrated very high quantum yields (up to 700%) for the formation of two or more electron−hole pairs per absorbed photon. Yet, subsequent studies[22,43] showed ultrafast intraband charge-phonon relaxation in PbSe QDs, suggesting that the phonon bottleneck is not required for an efficient carrier multiplication. Moreover, the relaxation was faster in smaller QDs. The observed carrier multiplication has great potential to enhance the efficiency of QD photovoltaic devices.[6] However, its mechanism and competition with the counterproductive phonon-induced charge relaxation are not well understood.

* Address correspondence to this author. E-mail: prezhdo@u.washington.edu.

10.1021/jp0669052 CCC: $37.00
Published on Web 03/07/2007

The current work presents the first time-domain ab initio simulation of the phonon-mediated electron and hole relaxation dynamics in a QD. The study details those particular features of the electron and hole relaxation in PbSe QDs which rationalize why carrier multiplication was first observed in this semiconductor. In particular, the simulation shows that the phonon bottleneck to the electron and hole relaxation does not exist. However, the relaxation is still relatively slow and nearly symmetric with respect to the band gap. The absence of the phonon bottleneck is explained by the relatively high densities of electron and hole states. While not all states are optically active, most of them facilitate the phonon-induced relaxation. The slight asymmetry in the electron and hole band structure is sufficient to allow symmetry-forbidden transitions that can be detected in the optical absorption or fluorescence spectra. The dynamics proceeds through multiple states at intermediate energies and is notably nonexponential, agreeing with the non-Lorentzian spectral line shapes.[18] The holes decay slightly faster than the electrons due to their higher state density. The difference in the hole and electron relaxation times is insignificant, such that Auger energy exchange between the charge carriers cannot speed up the overall relaxation. This is in contrast, for instance, to CdSe QDs, in which holes relax significantly faster than electrons, and electrons are able to lose energy through holes by Auger processes.[21] Both electrons and holes interact only with low-frequency phonons. As a result, the relaxation is several times slower than the observed carrier multiplication time.[6−11]

The theoretical background of the performed simulations is reviewed in the following section and is followed by a detailed analysis of the simulation results. The key results are summarized in the conclusions section within a broader perspective of photoinduced excitation dynamics in QDs.

2. Theory

The real-time atomistic ab initio simulation of the charge-phonon relaxation dynamics reported below was made possible by the recent implementation[44] of trajectory surface hopping (TSH)[45−47] within time-dependent Kohn−Sham (KS) theory.[48−50] TSH is a fully atomistic nonadiabatic molecular dynamics (NAMD) approach that satisfies detailed balance.[47] It is one of the most common NAMD schemes[44,51−57] and can be viewed as a quantum master equation for electron dynamics, where the state-to-state transition rates depend on time through coupling to explicit phonon dynamics.

2.1. Time-Dependent Density Functional Theory. The electron density in the time-dependent density functional theory (TDDFT) is written in the KS representation[48−50] as

$$\rho(x,t) = \sum_{p=1}^{N_e} |\varphi_p(x,t)|^2 \tag{1}$$

where N_e is the number of electrons and the $\varphi_p(x,t)$ are single-electron KS orbitals. The evolution of the $\varphi_p(x,t)$ is determined by application of the TD variational principle to the KS energy

$$E\{\varphi_p\} = \sum_{p=1}^{N_e}\langle\varphi_p|K|\varphi_p\rangle + \sum_{p=1}^{N_e}\langle\varphi_p|V|\varphi_p\rangle + \frac{e^2}{2}\frac{\int\int \rho(x',t)\rho(x,t)}{|x-x'|}\,d^3x\,d^3x' + E_{xc}\{\rho\} \tag{2}$$

The right-hand side of eq 2 gives the kinetic energy of noninteracting electrons, the electron−nuclear attraction, the Coulomb repulsion of density $\rho(x,t)$, and the exchange-correlation energy functional that accounts for the residual many-body interactions. Application of the variational principle leads to a system of single-particle equations[48−50]

$$i\hbar\frac{\partial\varphi_p(x,t)}{\partial t} = H(\varphi(x,t))\varphi_p(x,t), \quad p = 1, ..., N_e \tag{3}$$

where the Hamiltonian H depends on the KS orbitals. In the generalized gradient approximation[58] used for the present simulation, E_{xc} depends on both density and its gradient, and the Hamiltonian is written as

$$H = -\frac{\hbar^2}{2m_e}\nabla^2 + V_N(x) + e^2\int\frac{\rho(x')}{|x-x'|}\,d^3x' + V_{xc}\{\rho,\nabla\rho\} \tag{4}$$

Expanding the time-dependent $\varphi_p(x,t)$ in the adiabatic KS orbitals $\tilde{\varphi}_k(x;R)$

$$\varphi_p(x,t) = \sum_k^{N_e} c_{pk}(t)|\tilde{\varphi}_k(x;R)\rangle \tag{5}$$

the TDDFT eq 3 transforms to an equation of motion for the coefficients

$$i\hbar\frac{\partial}{\partial t}c_{pk}(t) = \sum_m^{N_e} c_{pm}(t)(\epsilon_m\delta_{km} + \mathbf{d}_{km}\cdot\dot{\mathbf{R}}) \tag{6}$$

The nonadiabatic (NA) coupling

$$\mathbf{d}_{km}\cdot\dot{\mathbf{R}} = -i\hbar\langle\tilde{\varphi}_k(x;R)|\nabla_{\mathbf{R}}|\tilde{\varphi}_m(x;R)\rangle\cdot\dot{\mathbf{R}} = -i\hbar\left\langle\tilde{\varphi}_k\left|\frac{\partial}{\partial t}\right|\tilde{\varphi}_m\right\rangle \tag{7}$$

arises from the dependence of the adiabatic KS orbitals on the nuclear trajectory, and is computed most easily from the right-hand side of eq 7.[46]

The time-dependence in TDDFT for electron−nuclear dynamics is due to ionic motion, making $V_N(x) \equiv V_N(x;\mathbf{R}(t))$ dependent on time through the nuclear trajectory $\mathbf{R}(t)$. The prescription for R(t) constitutes the quantum-backreaction problem. To define the backreaction, TSH uses a stochastic element that creates both classical trajectory branching[45] and detailed balance.[47] The former mimics the ability of quantum mechanical wavepackets to split and evolve in correlation with different electronic states. The latter is essential for relaxation and leads to thermodynamic equilibrium.

2.2. Fewest Switches Surface Hopping in the Kohn−Sham Representation. TSH requires an electronic basis. Classical trajectories correlate with the states of this basis and hop between the states. Preferably, the THS basis is formed of adiabatic states,[45−47] i.e., eigenstates of the Hamiltonian (4). While the adiabatic forces for ground- and excited-electronic states as well as the NA coupling between them can be calculated in TDDFT,[48−50] the NA coupling between excited electronic states has not yet been defined. In ref 44 TSH was performed in the zeroth order adiabatic basis, using Slater determinants formed of adiabatic KS orbitals. Here, we use a further approximation by going from the many-particle to the single-particle representation: THS is performed on the basis of the single-particle adiabatic KS orbitals. The single-particle representation is well-suited for studies of QDs, whose electronic structure is well represented by the independent electron and hole picture.

Quantum confinement effects in QDs ensure that the electron and hole kinetic energies dominate the electrostatic interaction. As a result, even the basic effective mass theory provides a good description of the QD electronic structure. Quantum confinement effects are particularly strong in PbSe and are evident in QDs whose size is comparable to or smaller than the PbSe exciton localization length $d = 46$ nm.[37]

TSH prescribes a probability for hopping between electronic states. The probability is explicitly time-dependent and is correlated with the ionic evolution. In the fewest switches TSH,[45] the probability to hop between states k and m within time interval dt equals

$$dP_{km} = \frac{b_{km}}{a_{kk}} dt \tag{8}$$

where

$$b_{km} = -2\mathrm{Re}(a^*_{km}\mathbf{d}_{km}\cdot\dot{\mathbf{R}}); \quad a_{km} = c_k c^*_m \tag{9}$$

Here, c_k and c_m are the coefficients evolving according to (6). The hopping probabilities explicitly depend on the NA coupling $\mathbf{d}_{km}\cdot\dot{\mathbf{R}}$ defined in eq 7. If the calculated dP_{km} is negative, the hopping probability is set to zero. This feature minimizes the number of hops: a hop from state k to state m can occur only when the electronic occupation of state k decreases and the occupation of state m increases. To conserve the total electron−nuclear energy after a hop, the nuclear velocities are rescaled[45,46] along the direction of the electronic component of the NA coupling $\mathbf{d}_{km}$. If a NA transition to a higher energy electronic state is predicted by eq 8, and the kinetic energy available in the nuclear coordinates along the direction of the NA coupling is insufficient to accommodate the increase in the electronic energy, the hop is rejected. The velocity-rescaling and hop-rejection give detailed balance between upward and downward transitions.[47]

The current, simplified implementation of TSH makes the assumption that the energy exchanged between the electronic and select nuclear degrees of freedom during the hop is rapidly redistributed between all nuclear modes. Under this assumption, the distribution of energy in the nuclear mode directed along the NA coupling $\mathbf{d}_{km}$ is Boltzmann at all times, and the velocity-rescaling plus hop-rejection can be replaced by multiplying the probability (8) for transitions upward in energy by the Boltzmann factor. Elimination of the velocity-rescaling gives great computational savings, avoiding explicit quantum-backreaction and allowing one to use a predetermined nuclear trajectory to evolve the electronic subsystem.

To recapitulate, the simplified version of fewest switches TSH is performed in the single-particle representation, with the hop-rejection replaced by multiplication of the TSH probability upward in energy by the Boltzmann factor. The NA electronic evolution (6) is performed by using the ground-state nuclear trajectory. This treatment of the electron and hole relaxation creates a sophisticated version of the quantum master equation with explicitly time-dependent transition probabilities that respond to nuclear evolution and give the correct short[59−61] and long-time dynamics.[45−47]

2.3. Simulation Details. We implemented the TSH theory with the VASP DFT package.[62] The simulations were performed with the Perdew and Wang exchange-correlation functional,[58] Vanderbilt pseudopotentials,[63] and a converged plane-wave basis. The simulations were carried out in a cubic cell periodically replicated in three dimensions, as stipulated by the plane-wave basis. To prevent spurious interactions between periodic images of the QD, the cell was constructed to have at least 8 Å of vacuum between the QD replicas.

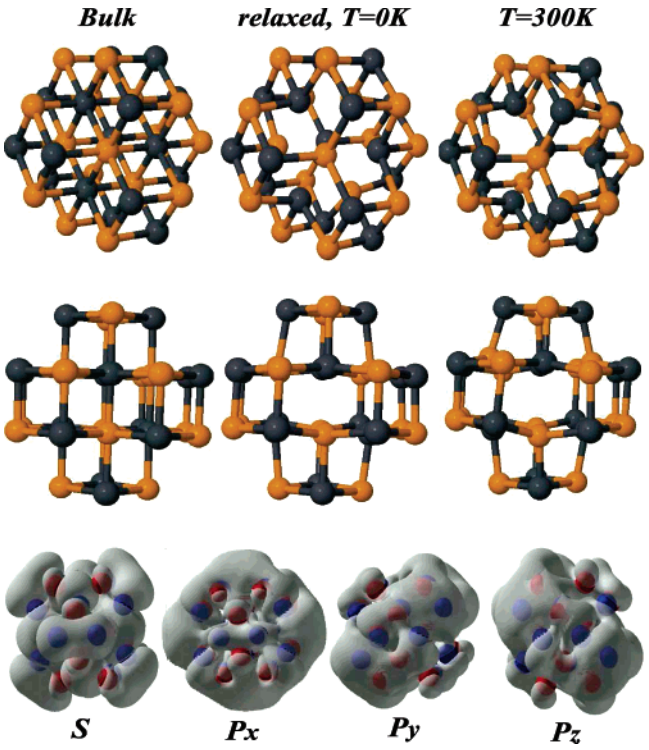

Figure 1. Geometric and electronic structure of the $Pb_{16}Se_{16}$ QD. The top and middle rows show the (110)- and (111)-surface views, respectively. Pb atoms are black and Se atoms are yellow. The 32-atom QD preserves the bulk topology, even though significant relaxation at 0 K relative to bulk and thermal fluctuations in the structure at room temperature are observed. The bottom row depicts the densities of the lowest excited electronic states, whose space symmetry characterizes them as S and P_x, P_y, P_z states.

The QD was initially constructed on a zinc-blend lattice of 16 atoms of Pb and 16 atoms of Se with bulk Pb−Se bond lengths at zero temperature, and then relaxed to its lowest energy configuration. This relaxed configuration was heated to 300 K and used for further dynamics calculations. Figure 1 compares the relaxed atomic geometries at zero and at room temperatures with the initial ideal zinc-blend bulk structure. Significant structural deformation of the QD due to relaxation was observed even at zero temperature. Temperature-induced fluctuations distort the dot further, but do not cause surface reorganization, or bond reconnectivity, preserving the bulk bonding topology, Figure 1. The diameter of the roughly spherical 32 atom PbSe nanocrystal is about 1 nm. Since PbSe is strongly ionic, its electronic properties are not strongly influenced by the surface structure,[37] and the surface was not passivated, creating substantial computational savings.

After the system was heated to 300 K by repeated velocity rescaling, a 4 ps microcanonical trajectory was performed in the ground-electronic state. The initial conditions for the NA dynamics were sampled from this trajectory. The transition dipole moments and oscillator strengths for excitations between KS orbitals were computed and used both to generate the optical absorption spectrum and to pick the most optically active excitations for the initial conditions of the NA runs. A 1 fs nuclear and a 10^{-3} fs electronic time step were used for the dynamics calculations. The data shown in the figures below are converged by averaging over 500 runs.

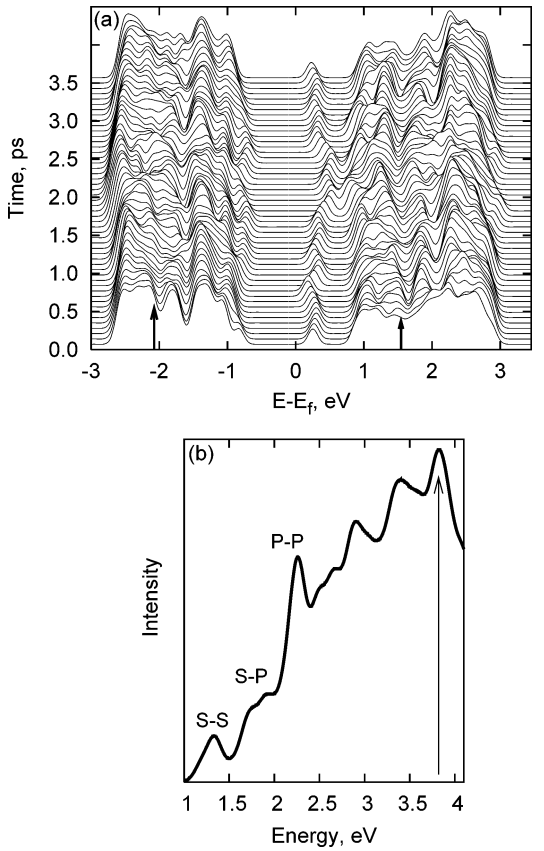

Figure 2. (a) Density of electron and hole states as a function of time along the MD run. The states show a moderate asymmetry across the gap, with the hole states having a slightly higher density. The arrows indicate the photoexcitation at the energy of three band gaps. (b) Electron absorption spectrum averaged over the MD run. The most pronounced peaks in the spectrum arise due to symmetric transitions across the gap, e.g., the S−S and P−P peaks. The spectrum also contains less pronounced, but nevertheless significant peaks due to asymmetric transitions, in particular the S−P peak.

3. Results

The reported state-of-the-art time-domain ab initio simulations of the charge relaxation processes in the PbSe QD provide novel and important details that were not accessible previously. In addition to the optimized geometries and electronic band structure which are available from the traditional simulations, the NA approach directly probes relaxation mechanisms and time scales, identifies phonon modes that are responsible for the relaxation, and allows for direct comparison with the corresponding time-resolved experimental data.

3.1. Electronic Structure and Optical Spectrum of the Quantum Dot. The electron densities of the four vacant orbitals closest to the edge of the CB are presented in the bottom panel of Figure 1. Their envelopes exhibit roughly S- and P-symmetries, which are significantly modified by the local atomic structure. This agrees with effective mass theory,[31,32] which represents the electron and hole wave functions as products of Bloch functions that vary on the atomistic level and S-, P-, D-, and so on envelope functions that encompass the whole QD and are eigenstates of particle in a spherical well. The S- and P-symmetries of the corresponding hole states at the edge of the VB are less pronounced.

The evolution of the density of states (DOS) of the PbSe cluster over a 3.5 ps time interval is presented in Figure 2a. The *z*-axis gives the state density as a function of energy and time. The calculated average energy gap of the 1 nm QD is 1.4 eV. As is typical with DFT, this value is likely underestimated, but it does follow the expected trend and exceeds the 1.25 eV gap observed for the smallest 1.4 nm QD studied experimentally.[22] The electronic structure and optical properties of bulk lead salts computed with a similar approach agree well with the experimental results.[64]

The shape of the calculated DOS follows the experimental data[22,42,43] and the ab initio tight-binding results.[65] The three main peaks on each side of the gap can be attributed to the expected S_e (S_h), P_e (P_h), and D_e (D_h) levels of electrons (holes). The separation of the S-state from the main manifold is more pronounced with the electrons than the holes, the latter having a slightly higher DOS. The difference in the electron and hole DOS for PbSe QDs is not nearly as dramatic as, for instance, for CdSe QDs.[18,21] The arrows in Figure 2a indicate the energies of electron and hole excitations, which are set to match three times the QD energy gap in correspondence with experiment.[9] For each nuclear configuration, the initially excited states are chosen based on the largest transition dipole moments among the states close to the energies indicated by the arrows. The similarity in the electron and hole state structure results in selection rules that favor symmetric photoexcitations across the gap.[37]

Figure 2b presents the optical absorption spectrum of the PbSe QD. As expected based on the selection rules, the strongest peaks in the spectrum correspond to symmetric transitions, e.g., S−S and P−P. Remarkably, the slight asymmetry in the electron and hole DOS, Figure 2a, is sufficient to allow asymmetric transitions, e.g., S−P, that also create strong optical bands. The asymmetric transitions can be less pronounced in larger clusters, since anisotropy of the small $Pb_{16}Se_{16}$ cluster shape can have a strong effect on the broken selection rules. Since the energy splitting between the S- and P-states is different for electrons and holes and is larger for the electrons, the S−P band contains two subpeaks. The lower energy one arises due to transitions between the P-states of holes and S-state of electrons. The higher energy subpeak creates excitations from the S-state of holes to the P-electronic states. The arrow in the spectrum figure indicates the simulated photoexcitation.

3.2. Active Phonon Modes. Figure 3 identifies the phonon modes that induce the relaxation of carriers to the edges of their bands. The figure shows Fourier transforms of the energies of the two most optically active initially exited electron and hole state pairs, as well as the highest occupied and lowest unoccupied molecular orbitals (HOMO/LUMO). The NA coupling is directly related to the second derivative of the energy along the nuclear trajectory[66] and, therefore, those vibrational modes that most strongly modulate the energy levels create the largest coupling. Figure 3 indicates that spheroidal acoustic phonons[37] with frequencies around 100 cm^{-1} dominate both electron and hole dynamics. The longitudinal optical modes with frequencies around 200 cm^{-1} are also clearly present in the influence spectra, but with a smaller amplitude. The result can be rationalized by the fact that the energy levels in the QD are more sensitive to the acoustic modes, which modulate QD size and shape, than to the optical modes with local atomic displacements, which tend to average out. The participation of the low-frequency phonons with zero-point energies around $k_BT/4$ at room temperature validates the classical-mechanical treatment of the nuclei.

Both amplitudes and frequencies of active phonon modes are similar for electrons and holes, suggesting that the relaxation dynamics of the two charge carriers in the PbSe QD should be similar. The spectrum is slightly broader for the electrons, Figure

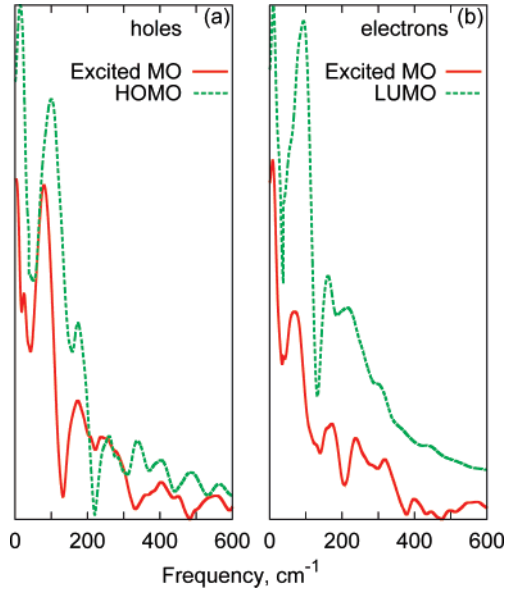

Figure 3. Fourier transforms of the energies of the initially photoexcited (solid lines) and band gap HOMO/LUMO (dashes) states of (a) holes and (b) electrons. Both charge carriers interact with low-frequency phonons, with electrons coupled to slightly faster phonons.

3b, and shows more higher frequency contributions compared to the spectrum of the holes, Figure 3a. This is to be expected, since the electron states are supported by higher energy KS orbitals, which contain more nodes, and therefore, couple more effectively to higher frequency vibrations that also have more nodes.[67] The participation of the faster modes should tend to speed the electron relaxation. However, this effect is counterbalanced by the lower density of electron states, Figure 2a. Which of the two factors contributes the most will be established by an analysis of the relaxation dynamics.

3.3. Phonon-Induced Electron and Hole Relaxation. The relaxation dynamics in the PbSe QD is detailed in Figures 4−6, and Table 1. Figure 4 presents energy relaxation of electrons and holes within the VB and CB, respectively. Part a shows a three-dimensional plot of the product of DOS with the state occupations as a function of energy and time. As evidenced by the data, the carriers visit multiple states during the relaxation, but none of the intermediate states play any special role. Comparing the DOS of Figure 2a with the population dynamics shown in Figure 4a, one observes for both electrons and holes that the initial photoexcitation peak vanishes, only to reappear at the final states. A slightly faster decay of holes compared to electrons is seen in the average electron and hole energies, Figure 4b. The average energy of both electrons and holes plateaus after 1.5 ps. However, while the average hole energy is nearly equal to the HOMO energy, the average electron energy is between the LUMO and LUMO+1 energies. By 3 ps, 95% of holes have reached the HOMO, and only 70% of electrons have populated the LUMO, demonstrating that the charge-carrier relaxation contains an additional slower component that cannot be fully resolved over the simulation time scale.

Figure 5 shows the probability−density distributions for the electron and hole transitions as a function of the transition energy. The transitions occur both up and down in energy; however, transition downward dominate, as required by the detailed balance. The overall energy flow from the charged particles to phonons is responsible for the relaxation of the initial photoexcitation. While the most likely transitions involve small amounts of energy, up to 1 eV of electron and hole energy can occasionally be lost in a single event. The majority of the transitions result in exchange of energy that exceeds the energy of a single phonon, which is around 200 $cm^{-1} \approx 0.025$ eV,

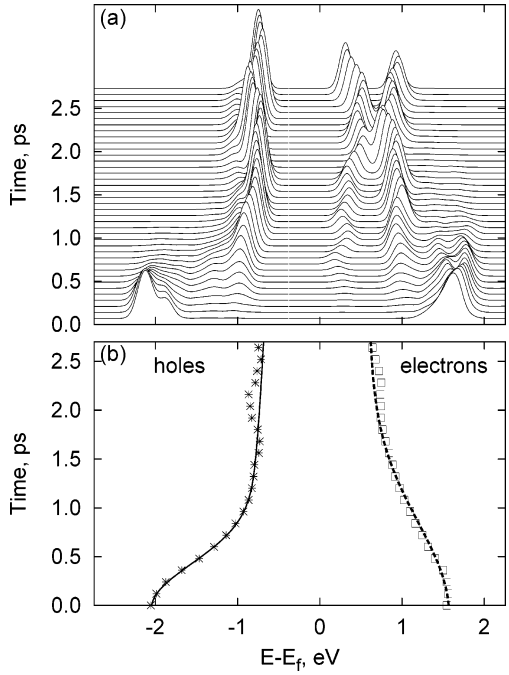

Figure 4. Relaxation dynamics of electrons and hole energies. (a) Electron and hole energy distributions computed by multiplying the DOS (see Figure 3a) by the corresponding state occupations, and averaging over 500 initial conditions. The major part of the relaxation occurs within the first picosecond. A slower relaxation component associated with relaxation all the way to the band gap states occurs on a slower time scale, as seen particularly well with the gradual growth of the lowest electronic state population. (b) Average energies (symbols). The time scales of the fit (lines) are presented in Table 1.

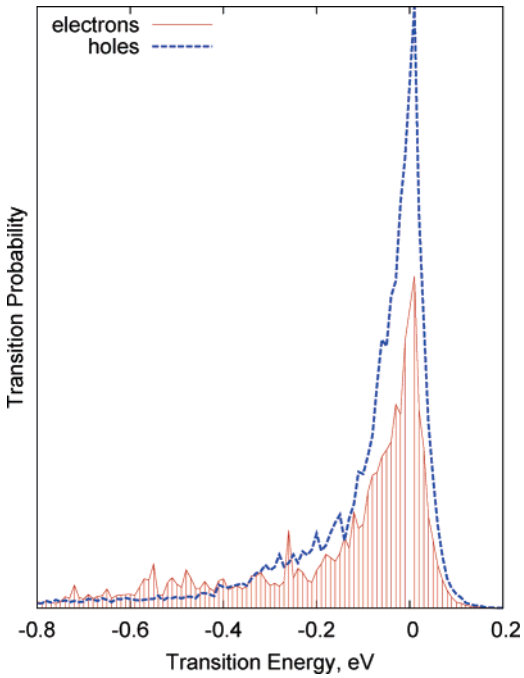

Figure 5. Probability density of the electron and hole transitions as a function of the transition energy. While most hops occur down in energy and are responsible for the charge-phonon relaxation, some hops transfer energy from phonons to the charged particles. The energy exchanged during most of the transitions is greater than the characteristic phonon energy of 200 $cm^{-1} \approx 0.025$ eV, Figure 3, characterizing these transitions as multiphonon.

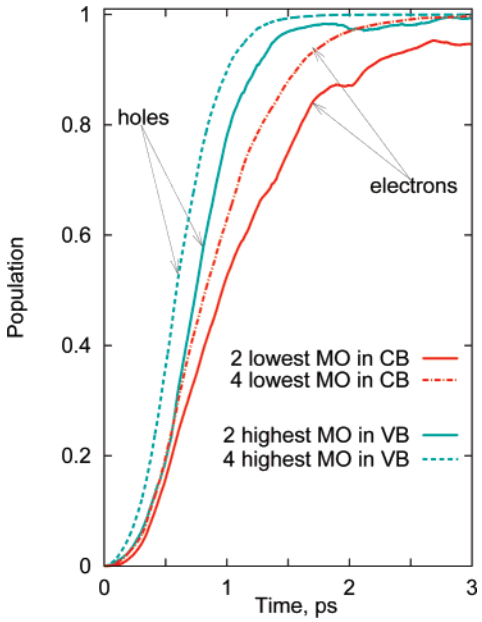

Figure 6. Time-dependent populations of the 2 and 4 states of electrons and holes nearest to the band gap edge. The holes evolve only slightly faster than the electrons.

TABLE 1: Parameters of the Gaussian Plus Exponential Fit, Eq 10, to the Average Electron and Hole Energies Shown in Figure 4b

	τ_G, ps	τ_{exp}, ps	A_G	E_i, eV	E_f, eV
holes	0.45	2.7	0.70	−2.04	−0.52
electrons	0.80	2.7	0.75	1.57	0.52

Figure 3. Therefore, the charge-phonon relaxation in the PbSe QD occurs primarily via the multiphonon mechanism.[22,43] The transition probability−density distribution is sharper for the holes than for the electrons. This correlates with the facts that holes couple more strongly to lower frequency phonons, Figure 3, and therefore can exchange less energy than electrons in an equivalent multiphonon transition.

The time-dependent occupations of the first 2 and 4 band gap states of electrons and holes are shown in Figure 6. By the end of the simulation, nearly all of the holes are relaxed into the highest two states of the VB. As for the electrons, a substantial fraction of them, about 7%, still exist above the 2 lowest states of the CB. Only when all 4 states of the S- and P-state manifolds are included can the relaxation be considered complete by 3 ps.

The relaxation of the electron and hole energies shown in Figure 4b is not exponential, which agrees with the strongly non-Lorentzian line shapes observed experimentally.[18] Note that standard master-equation treatments[68] with constant transition rates give exponential relaxation. The nonexponential profile of the energy decay present in the current simulation is due to the explicit time-dependence of the relaxation rates provided by TSH.[44−47] TSH correctly represents the vanishing time-derivative of the quantum-mechanical transition probability at zero time, which is manifested in the quantum-Zeno effect[59−61] and gives the Gaussian relaxation component at early times.

The average energies, Figure 4b, are fit well by the sum of the fast Gaussian and slow exponential components

$$E(t) = (E_i - E_f)\{A_G \exp[-0.5(t/\tau_G)^2] + (1 - A_G)\exp[-t/\tau_{exp}]\} + E_f \quad (10)$$

The fit parameters are presented in Table 1. The initial Gaussian component provides 70% and 75% of the hole and electron relaxation amplitude, respectively, and dominates the overall relaxation for both carriers. The relaxation time scales are determined by several factors, including DOS, whose high magnitude favors relaxation, the charge-phonon coupling, which is quite similar for electrons and holes, and the active phonon mode frequencies, which determine how fast the phonons can respond to charge carriers. Even though electrons couple better to higher frequency phonons, Figure 3, they have a smaller DOS, Figure 2a. The DOS factor wins, and the electron energy decays more slowly than the hole energy, Table 1.

The calculated 450−800 fs Gaussian and 2.7 ps exponential components of the charge-phonon relaxation are in good agreement with the measured subpicosecond to picosecond times, which become faster for smaller QDs.[22,43] The reported results indicate that the phonon bottleneck to the electron and hole relaxation occurs only at the last stages of the simulated relaxation, and even then mostly for the electrons. The absence of the bottleneck in the initial relaxation is associated with a relatively dense spacing of the electron and hole states at higher energies. Except for the two lowest energy states of the CB, the typical spacing between the photoexcited state and its nearest neighbors nearly matches the phonon frequencies. Still, even the initial Gaussian relaxation is at least twice slower than the charge carrier multiplication time with an observed upper bound of 250 fs.[7,10,11]

4. Discussion and Conclusions

For the first time, we have simulated the phonon-mediated electron and hole dynamics in a QD by ab initio TDDFT in real time and at the atomistic level of detail. The calculated relaxation time scales agree with the direct experimental data[22,43] showing subpicosecond to several picosecond relaxation that becomes faster in smaller QDs. In our simulation of a small dot, the bulk of the relaxation occurs within 0.45−0.8 ps. The minor 2.7 ps component seen at the final stage of the relaxation is due to the small size of the simulated QD creating wide gaps between the first and second band edge states, particularly for the electron. The simulated 0.45−0.8 ps relaxation also agrees with the experimental detection of charge carrier multiplication that occurs within 0.25 ps and successfully competes with the relaxation.[7−11]

The atomistic picture provided by the reported simulation unifies the two, seemingly contradicting experimental observations of the large line spacing in the optical spectra of QDs and the absence of the phonon bottleneck. The fast charge-phonon relaxation and, therefore, the absence of the phonon bottleneck are attributed to a relatively high density of electron and hole states. The spacing between the state energies nearly matches the phonon frequencies, in contrast to the common view that the quantum confinement results in strong quantization of electronic energy levels in QDs. While the optical absorption spectrum indeed shows discrete bands that can be attributed to S−S, P−P, etc. excitations between hole and electron states, as described in the effective mass theory,[31,32] each band is composed of multiple transitions between pairs of hole and electron states. There is no contradiction between the effective mass and ab initio results. The optical selection rules, which are clearly defined in the effective mass approach, are also seen in the ab initio calculation, in which most of the states are weakly optically active. In contrast to the optical selection rules, which are determined by the *x*, *y*, and *z* light polarization components, the electron−phonon coupling selection rules are much more relaxed. Multiple phonons of various symmetries

couple most of the electronic states, facilitating the nonradiative relaxation. Although not all states are equally optically active, the majority of them take part in the relaxation.

The band structure of the PbSe QD is relatively symmetric with respect to the band gap. As a result, the electrons and holes relax on similar time scales. The slight asymmetry in the band structure is sufficient to break the optical selection rule that stipulates symmetric transitions, e.g., S−S and P−P. The asymmetric excitations between the valence and conduction bands, such as S−P and P−S, create additional bands in the optical absorption spectrum. Although these bands are not as strong as the symmetric bands, they are significant and can be detected experimentally. The S−P and P−S transitions occur at different energies owing to the slightly higher density of VB states relative to the CB. The somewhat higher hole DOS provides more relaxation pathways, resulting in a slightly faster relaxation of holes compared to electrons. This small difference in the electron and hole relaxation renders inefficient the hole-assisted Auger relaxation pathway. The latter is seen, for instance, in CdSe QDs, in which holes relax significantly faster than electrons, and electrons lose their energy by transferring it to holes.[21] The highly nonexponential profile of simulated energy decay agrees with the strongly non-Lorentzian spectral line shapes observed experimentally.

The relaxation occurs through NA charge−phonon interactions. Both charge carriers interact more strongly with acoustic than with optical phonons. This is because the NA coupling is directly related to the second derivative of the energy, and the latter is more sensitive to acoustic modes that modulate the shape and size of the dot and less sensitive to optical modes, whose effect on the energy tends to average out over the multiple bulk semiconductor unit cells that form the QD. The electrons interact slightly better with optical modes, as can be rationalized by the better match between the nodal structure of the CB states and optical modes.[67] Both are higher in energy, and therefore have more nodes than the VB states and acoustic modes, respectively. Even though the coupling of electrons to faster phonons should speed up electron relaxation, this effect is minor and is dominated by the lower electron DOS that explains why electrons relax more slowly than holes. The energy exchanged between the charged particles and phonons during the majority of the transitions is greater than the energy of a single phonon quantum, indicating that the transitions occur by the multiphonon mechanism. On average, less energy is exchanged per transition with the holes than the electron, because both the spacing between the hole states is smaller and the holes couple more strongly to lower frequency phonons.

The computational expense of the simulation limits the reported study to a small 32 atom PbSe QD, which, however, gives a good representation of larger QDs. The 32 atom cluster preserves the bulk topology and is not an amorphous collection of atoms. Therefore, it belongs to the same type of material as the larger dots. Surface states created by unsaturated bonds are not as important in PbSe as in other semiconductors, such as CdSe. Although the surface relaxation and the shape asymmetry should be less pronounced in larger QDs, the high state degeneracy of an ideal spherical potential is still lifted in larger dots due to disorder generated by thermally activated phonon modes. Consider the following order of magnitude estimate of the expected state degeneracy in a large QD composed of 1 000 atoms. Pb and Se atoms contain 14 and 6 valence electrons, respectively, averaging 10 per atom. Therefore, a 1 000 atom PbSe QD has 10 000 valence electrons. Assuming that these electrons create delocalized states that span 10 eV in energy, an average spacing between the states must be on the order of 0.001 eV. To produce energy gaps of around 0.1 eV seen in the optical spectra, the single particle electron and hole states must be 100-fold degenerate on average. The number of two-particle electron−hole excitations is $(10\,000)^2 = 100\,000\,000$, requiring an enormous degeneracy in order to create a 0.1 eV state spacing. The energy of thermal phonon motions is $kT_B = 0.025$ eV at room temperature. Lifting the degeneracy, the thermal disorder creates a multitude of closely spaced states that prevents the phonon bottleneck.

The details provided by the reported simulations generate valuable insights into the QD properties, reconcile the seemingly contradicting observations of wide optical line spacing and no phonon bottleneck to the relaxation, and rationalize why the highly efficient carrier multiplication is possible in PbSe nanocrystals despite the absence of the phonon bottleneck.

Acknowledgment. The authors are grateful to Dr. Kiril Tsemekhman for fruitful discussions. This research was supported by grants from the DOE (no. DE-FG02-05ER15755) and the ACS PRF (no. 41436-AC6).

References and Notes

(1) Milliron, D. J.; Hughes, S. M.; Cui, Y.; Manna, L.; Li, J. B.; Wang, L. W.; Alivisatos, A. P. *Nature* **2004**, *430*, 190.
(2) Ouyang, M.; Awschalom, D. D. *Science* **2003**, *301*, 1074.
(3) Gorman, J.; Hasko, D.; Williams, D. *Phys. Rev. Lett.* **2005**, *95*, 090502.
(4) Petta, J.; Johnson, A.; Taylor, J.; Laird, E.; Yacoby, A.; Lukin, M.; Marcus, C.; Hanson, M.; Gossard, A. *Science* **2005**, *309*, 2180.
(5) Scheibner, R.; Buhmann, H.; Reuter, D.; Kiselev, M.; Molenkamp, L. *Phys. Rev. Lett.* **2005**, *95*, 176602.
(6) Nozik, A. J. *Annu. Rev. Phys. Chem.* **2001**, *52*, 193.
(7) Ellingson, R. J.; Beard, M. C.; Johnson, J. C.; Yu, P. R.; Micic, O. I.; Nozik, A. J.; Shabaev, A.; Efros, A. L. *Nano Lett.* **2005**, *5*, 865.
(8) Murphy, J. E.; Beard, M. C.; Norman, A. G.; Ahrenkiel, S. P.; Johnson, J. C.; Yu, P.; Micic, O. I.; Ellingson, R. J.; Nozik, A. J. *J. Am. Chem. Soc.* **2006**, *128*, 3241.
(9) Schaller, R. D.; Klimov, V. I. *Phys. Rev. Lett.* **2004**, *92*, 186601.
(10) Schaller, R. D.; Agranovich, V. M.; Klimov, V. I. *Nature Phys.* **2005**, *1*, 189.
(11) Schaller, R. D.; Sykora, M.; Pietryga, J. M.; Klimov, V. I. *Nano Lett.* **2006**, *6*, 424.
(12) Klimov, V. I. *J. Phys. Chem. B* **2006**, *110*, 16827.
(13) Klimov, V. I.; Mikhailovsky, A. A.; Xu, S.; Malko, A.; Hollingsworth, J. A.; Leatherdale, C. A.; Eisler, H. J.; Bawendi, M. G. *Science* **2000**, *290*, 314.
(14) Talapin, D.; Murray, C. *Science* **2005**, *310*, 86.
(15) Coe, S.; Woo, W.; Bawendi, M.; Bulovic, V. *Nature* **2002**, *420*, 800.
(16) Farahani, J.; Pohl, D.; Eisler, H.; Hecht, B. *Phys. Rev. Lett.* **2005**, *95*, 017402.
(17) Dahan, M.; Levi, S.; Luccardini, C.; Rostaing, P.; Riveau, B.; Triller, A. *Science* **2003**, *302*, 442.
(18) Califano, M.; Zunger, A.; Franceschetti, A. *Annu. Rev. Phys. Chem.* **2001**, *52*, 193.
(19) Rumbles, G.; Selmarten, D. C.; Ellingson, R. J.; Blackburn, J. L.; Yu, P. R.; Smith, B. B.; Micic, O. I.; Nozik, A. J. *J. Photochem. Photobiol., A* **2001**, *142*, 187.
(20) Crooker, S.; Hollingsworth, J.; Tretiak, S.; Klimov, V. *Phys. Rev. Lett.* **2002**, *89*, 186802.
(21) Klimov, V.; Mikhailovsky, A.; McBranch, D.; Leatherdale, C.; Bawendi, M. *Science* **2000**, *287*, 1011.
(22) Schaller, R. D.; Pietryga, J. M.; Goupalov, S. V.; Petruska, M. A.; Ivanov, S. A.; Klimov, V. I. *Phys. Rev. Lett.* **2005**, *95*, 196401.
(23) Yu, P.; Nedeljkovic, J. M.; Ahrenkiel, P. A.; Ellingson, R. J.; Nozik, A. J. *Nano Lett.* **2004**, *4*, 1089.
(24) Johnson, A.; Petta, J.; Taylor, J.; Yacoby, A.; Lukin, M.; Marcus, C.; Hanson, M.; Gossard, A. *Nature* **2005**, *435*, 925.
(25) Schleser, R.; Ihn, T.; Ruh, E.; Ensslin, K.; Tews, M.; Pfannkuche, D.; Driscoll, D.; Gossard, A. *Phys. Rev. Lett.* **2005**, *94*, 206805.
(26) Peterson, J. J.; Krauss, T. D. *Nano Lett.* **2006**, *6*, 510.
(27) Semenov, Y.; Kim, K. *Phys. Rev. Lett.* **2004**, *92*, 026601.
(28) Wilson-Rae, I.; Zoller, P.; Imamoglu, A. *Phys. Rev. Lett.* **2004**, *92*, 075507.

(29) Muljarov, E.; Takagahara, T.; Zimmermann, R. *Phys. Rev. Lett.* **2005**, *95*, 177405.
(30) Kamisaka, H.; Kilina, S. V.; Yamashita, K.; Prezhdo, O. V. *Nano Lett.* **2006**, *6*, 2295.
(31) Efros, A. L.; Efros, A. L. *Sov. Phys. Semicond.* **1982**, *16*, 772.
(32) Brus, L. E. *J. Chem. Phys.* **1984**, *80*, 4403.
(33) Puzder, A.; Williamson, A. J.; Gygi, F.; Galli, G. *Phys. Rev. Lett.* **2004**, *92*, 217401.
(34) Zhou, Z. Y.; Brus, L.; Friesner, R. *Nano Lett.* **2003**, *3*, 163.
(35) Califano, M.; Zunger, A.; Franceschetti, A. *Nano Lett.* **2004**, *4*, 525.
(36) He, L. X.; Bester, G.; Zunger, A. *Phys. Rev. Lett.* **2005**, *94*, 016801.
(37) Wise, F. W. *Acc. Chem. Res.* **2000**, *33*, 773.
(38) Wehrenberg, B. L.; Wang, C. J.; Guyot-Sionnest, P. *J. Phys. Chem. B* **2002**, *106*, 10634.
(39) Zeng, H. Z.; Schelly, Z. A.; Ueno-Noto, K.; Marynick, D. S. *J. Phys. Chem. A* **2005**, *109*, 1616.
(40) Lu, W. G.; Fang, J. Y.; Ding, Y.; Wang, Z. L. *J. Phys. Chem. B* **2005**, *109*, 19219.
(41) Peterson, J. J.; Krauss, T. D. *Phys. Chem. Chem. Phys.* **2006**, *8*, 3851.
(42) Liljerothos, P.; van Emmichoven, P. A. Z.; Hickey, S. G.; Weller, H.; Grandidier, B.; Allan, G.; Vanmaekelbergh, D. *Phys. Rev. Lett.* **2005**, *95*, 086801.
(43) Harbold, J. M.; Du, H.; Krauss, T. D.; Cho, K. S.; Murray, C. B.; Wise, F. W. *Phys. Rev. B* **2005**, *72*, 195312.
(44) Craig, C. F.; Duncan, W. R.; Prezhdo, O. V. *Phys. Rev. Lett.* **2005**, *95*, 163001.
(45) Tully, J. C. *J. Chem. Phys.* **1990**, *93*, 1061.
(46) Hammes-Schiffer, S.; Tully, J. C. *J. Chem. Phys.* **1994**, *101*, 4657.
(47) Parahdekar, P. V.; Tully, J. C. *J. Chem. Phys.* **2005**, *122*, 094102.
(48) Marques, M. A. L.; Gross, E. K. U. *Annu. Rev. Phys. Chem.* **2004**, *55*, 427.
(49) Baer, R.; Neuhauser, D. *J. Chem. Phys.* **2004**, *121*, 9803.
(50) Tretiak, S.; Igumenshchev, K.; Chernyak, V. *Phys. Rev. B* **2005**, *71*, 033201.
(51) Li, X. S.; Tully, J. C.; Schlegel, H. B.; Frisch, M. J. *J. Chem. Phys.* **2006**, *123*, 084106.
(52) Tully, J. C. In *Classical and Quantum Dynamics in Condensed Phase Simulations*; Berne, B. J., Ciccotti, G., Coker, D. F., Eds.; World Scientific: Singapore, 1998; pp 489−514.
(53) Coker, D. F. In *Computer Simulations in Chemical Physics*; Allen, M. P., Tildesley, D. J., Eds.; Kluwer Academic Publishers: Dordrecht, The Netherlands, 1993; pp 315−377.
(54) Prezhdo, O. V.; Rossky, P. J. *J. Chem. Phys.* **1997**, *107*, 825.
(55) Prezhdo, O. V. *J. Chem. Phys.* **1999**, *111*, 8366.
(56) Prezhdo, O. V.; Brooksby, C. *Phys. Rev. Lett.* **2001**, *86*, 3215.
(57) Prezhdo, O. V. *Theor. Chem. Acc.* **2006**, *116*, 206.
(58) Perdew, J. P. In *Electronic Structure of Solids*; Ziesche, P., Eschrig, H., Eds.; Akademie Verlag: Berlin, Germany, 1991.
(59) Prezhdo O. V.; Rossky, P. J. *Phys. Rev. Lett.* **1998**, *81*, 5294.
(60) Prezhdo, O. V. *Phys. Rev. Lett.* **2000**, *85*, 4413.
(61) Luis, A. *Phys. Rev. A* **2003**, *67*, 062113.
(62) Kresse, G.; Furthmüller, J. *Comput. Mater. Sci.* **1996**, *6*, 15.
(63) Vanderbilt, D. *Phys. Rev. B* **1990**, *41*, 7892.
(64) Albanesi, E. A.; Blanca, E. L. P. Y.; Petukhov, A. G. *Comput. Mater. Sci.* **2005**, *32*, 85.
(65) Allan, G.; Delerue, C. *Phys. Rev. B* **2004**, *70*, 245321.
(66) Miller, W. H.; George, T. F. *J. Chem. Phys.* **1972**, *56*, 5637.
(67) Habenicht, B. F.; Craig, C. F.; Prezhdo, O. V. *Phys. Rev. Lett.* **2006**, *96*, 187401.
(68) Kondov, I.; Kleinekathofer, U.; Schreiber, M. *J. Chem. Phys.* **2003**, *119*, 6635.